Loughborough University

Loughborough University
Institutional Repository

# *Frequency range of stable dielectric-barrier discharges in atmospheric He and N2*

This item was submitted to Loughborough University's Institutional Repository by the/an author.

**Citation:** DENG, X.T. and KONG, M.G., 2004. Frequency range of stable dielectric-carrier discharges in atmospheric He and N2. IEEE Transactions on Plasma Science, 32(4), pt.3, pp.1709-1715.

**Additional Information:**

- This article was published in the journal, IEEE Transactions on Plasma Science [© 2004 IEEE] and is also available at: http://ieeexplore.ieee.org/ Personal use of this material is permitted. However, permission to reprint/republish this material for advertising or promotional purposes or for creating new collective works for resale or redistribution to servers or lists, or to reuse any copyrighted component of this work in other works must be obtained from the IEEE.

**Metadata Record:** https://dspace.lboro.ac.uk/2134/5223

**Version:** Published

**Publisher:** © IEEE

Please cite the published version.

Loughborough University

This item was submitted to Loughborough's Institutional Repository (https://dspace.lboro.ac.uk/) by the author and is made available under the following Creative Commons Licence conditions.

creative commons

COMMONS DEED

**Attribution-NonCommercial-NoDerivs 2.5**

**You are free:**

- to copy, distribute, display, and perform the work

**Under the following conditions:**


**Attribution**. You must attribute the work in the manner specified by the author or licensor.

**Noncommercial**. You may not use this work for commercial purposes.

**No Derivative Works**. You may not alter, transform, or build upon this work.

- For any reuse or distribution, you must make clear to others the license terms of this work.
- Any of these conditions can be waived if you get permission from the copyright holder.

**Your fair use and other rights are in no way affected by the above.**

This is a human-readable summary of the Legal Code (the full license).

Disclaimer

For the full text of this licence, please go to:
http://creativecommons.org/licenses/by-nc-nd/2.5/

# Frequency Range of Stable Dielectric-Barrier Discharges in Atmospheric He and $N_2$

Xu Tao Deng, *Student Member, IEEE,* and Michael G. Kong, *Senior Member, IEEE*

***Abstract*—While there have been extensive studies of nonthermal atmospheric dielectric-barrier discharges (DBD), many key facets of their characteristics remain to be unraveled before their full understanding is achieved. One of the missing pieces in our current knowledge is the dependence of stable DBD production upon temporal characteristics of the applied voltage such as excitation frequency. In this contribution, we report a numerical investigation of the frequency range for the generation of stable DBD and that of likely mechanisms for disruption of DBD stability. We show that when the excitation frequency is too low, an irreversibly large mismatch of the rise-time occurs between the applied voltage and the memory voltage. It is demonstrated that this mismatch results in a rapid suppression of the gas voltage and as such, the generated DBD is quenched prematurely. Also, it is shown that when the excitation frequency is too high, most electrons produced in the plasma bulk become trapped in the interelectrode gap and are unable to reach the electrodes. As a result, the gas voltage increases without being contained adequately by a sizeable memory voltage. Again, this leads to premature plasma quenching. These observations highlight the importance of the dynamic balance between the applied voltage and the memory voltage in dielectric-barrier discharges. We compare the above issues in both a helium DBD and a nitrogen DBD and report that our findings of the two stability disruption mechanisms are generic in different DBD systems.**

***Index Terms*—Atmospheric pressure nonthermal plasmas, frequency mechanisms, gas discharge, plasma modeling, stability.**

## I. Introduction

NONTHERMAL atmospheric glow discharges have recently become an important subject of plasma research due to their increasing applications in key areas of material processing, biological decontamination, and pollution control [1], [2]. One such nonthermal atmospheric plasma is the dielectric-barrier discharges (DBD), generated between dielectrically insulated electrodes and typically at audio frequencies. The role of the dielectric coatings on the electrodes is to allow electrons to accumulate dynamically on the electrodes and, as such, to allow the accumulating electrons to form an opposing electric field to the applied field in each half cycle of the latter [3]–[7]. This opposing field is crucial in preventing glow-to-arc transition that is often inevitable at atmospheric pressure. Experimental and numerical studies of DBD have so far established their current-voltage characteristics, plasma dynamics, and density range of charged particles [3]–[7]. Some aspects of plasma chemistry are also examined by investigating, for example, the effect of a small nitrogen content in predominantly helium plasmas [3], [7]. These studies are particularly important in advancing the current knowledge of atmospheric dielectric-barrier discharges. Yet, an in-depth understanding of the fundamental plasma processes in the generation and operation of stable atmospheric DBD is still far from complete.

One of the missing pieces in a full understanding of atmospheric DBD is the dependence of their stable production upon temporal characteristics of the applied voltage such as excitation frequency and waveform [5]–[7]. A sound understanding of this correlation will offer valuable insight into the fundamental mechanisms of stable DBD generation. It will also establish the frequency range in which atmospheric DBDs are most stable and hence most appropriate for wide-ranging applications. Although stable atmospheric DBD have been generated experimentally at different and discrete frequencies of sinusoidal excitation [5], [6], a generic frequency dependence of stable DBD generation enables a capability of significant practical implications. For example, it will allow informed choice of power sources from commercial products for DBD production and facilitate design considerations for optimized and future power sources. Ultimately, this generic dependence will contribute to system optimization of atmospheric dielectric-barrier discharge equipment with tailored characteristics for DBD dynamics and for power source matching.

An experimental study of the frequency range of stable DBD requires either many fixed-frequency power sources or several less-optimized variable-frequency sources to cover as wide a frequency range as possible. This is an expensive approach particularly because the targeted frequency range is unknown at the outset of such study and multiple power sources have to be sourced. In this contribution, we use a recently developed computer code [7] to establish numerically the frequency range for the generation of stable DBD and to explore likely mechanisms for disruption of DBD stability. It will be shown that at a too low excitation frequency accumulating electrons on the dielectric coatings set up too quickly the opposing electric field and, as such, overly suppress the growth of the applied voltage. This results in a premature quenching of atmospheric DBD. When the excitation frequency is too high on the other hand, electrons generated in the plasma bulk become trapped within the interelectrode space and, as such, are unable to reach the electrodes to form the necessary opposing electric field. Similarly, this also disrupts the stability of the DBD and leads to plasma quenching. We investigate the above issues for two different atmospheric dielectric-barrier discharges; namely impure helium DBD (helium mixed with a fraction of nitrogen) and pure nitrogen DBD. The comparison of results for these two different DBD will establish whether our results are generic with different plasma chemistry in action.

Manuscript received August 8, 2003; revised December 9, 2003.

The authors are with the Department of Electronic and Electrical Engineering, Loughborough University, Leicestershire LE11 3TU, U.K. (e-mail: m.g.kong@lboro.ac.uk).

Digital Object Identifier 10.1109/TPS.2004.831599

0093-3813/04$20.00 © 2004 IEEE

Authorized licensed use limited to: LOUGHBOROUGH UNIVERSITY. Downloaded on August 26, 2009 at 09:23 from IEEE Xplore. Restrictions apply.

## II. Numerical Model

Atmospheric dielectric-barrier discharges are generated between two dielectrically coated parallel-plate electrodes and usually with a sinusoidal excitation voltage. To date, their numerical simulation has been based on hydrodynamic models that assume equilibrium between electrons and the local electric field [3], [6], [7]. Whereas electrons may not always be in equilibrium with the local electric field in parts of the interelectrode space (such as cathode sheath), hydrodynamic models have accurately predicted the experimentally measured discharge current and voltage [3], [7]. Therefore, they are realistic tools to study atmospheric DBD and this is confirmed recently through a comparison between hydrodynamic models and a kinetic model for atmospheric dc glow discharges [8]. For this reason, a hydrodynamic model will be used for our study here.

We will give only a brief introduction to our hydrodynamic model here since its details are provided elsewhere [7]. The ionized gas of atmospheric DBD is treated as a fluid whose dynamics is in principle governed by Boltzmann's equations describing species density, momentum, and energy conservation. Because of the short energy relaxation time of electrons in atmospheric-pressure discharges, the local field approximation is used [9]. Under this hydrodynamic approximation, the energy transfer equations for electrons and ions are ignored, thus simplifying the model to have only the continuity and momentum transfer equations. As a result, the transport parameters can be expressed as a function of the reduced local electric field, $E/N$, only [3], [6]–[9]. The electric field in the space between two electrodes has two components: one induced by the externally applied voltage and the other by space charges. Poison's equation is then added for the calculation of the electric field, and the numerical algorithm used to solve this set of equations is essentially based on the Patankar scheme [10]. Our numerical model is one-dimensional and accounts for spatial variation in the direction of the electrode axis (e.g., perpendicular to the electrode surface). Also, it assumes spatial uniformity in any direction that is parallel to the two electrodes.

For atmospheric DBD in helium mixed with a small amount of nitrogen (say 0.5%), Penning ionization is important [3], [7]. To this end, our model considers 9 species; namely electrons, atomic helium ions ($\mathrm{He}^+$), molecular helium ions ($\mathrm{He}_2^+$), molecular nitrogen ions ($\mathrm{N}_2^+$), atomic helium metastables ($\mathrm{He}(2^3\mathrm{S})$ and $\mathrm{He}(2^1\mathrm{S})$), molecular helium metastables ($\mathrm{He}_2^*$), and two ground-state neutral species He atoms and $\mathrm{N}_2$ molecules. The reactions among these species include direct ionization, excitation, de-excitation, Penning ionization, stepwise ionization, charge transfer, and recombination [7]. Furthermore, we consider secondary electron emission from the two electrodes caused by ion bombardment. In literature, the secondary emission rate for helium ions varies from 0.01 [11], [12] to 0.2 [9], [13] depending on bombarding species and electrode properties. For this study, we choose 0.1 as a representative figure [14]. The breakdown voltage can be calculated from

$$\gamma(e^{\alpha d} - 1) = 1 \tag{1}$$

where $\alpha$ and $\gamma$ are respectively Townsend's first and second ionization coefficients (or secondary electron emission rate). For helium, $\alpha$ is given by [13]

$$\alpha = Ap \exp\left(-B\sqrt{\frac{p}{E}}\right) \tag{2}$$

where $A = 4.4\ \mathrm{cm}^{-1}\mathrm{torr}^{-1}$ and $B = 14\ \mathrm{V}^{1/2}\mathrm{cm}^{-1/2}\mathrm{torr}^{-1/2}$. So across a helium gap of 0.5 cm the breakdown voltage is 1737 V, higher than experimental breakdown voltage of 1550 V [3].

The reactor considered here for helium DBD consists of two round parallel-plate electrodes of 2 cm radius and with a separation distance of 0.5 cm. Each electrode is coated with one thin layer of alumina of 0.06 cm thick, and we choose the relative permittivity for alumina to be 9 in our model. An external sinusoidal voltage source of 2 kV peak and 30 kHz is applied to the plasma reactor, and at 0.5% nitrogen content, the current and voltage characteristics of a helium-nitrogen discharge are shown in Fig. 1. This is very similar to that obtained in a comparable experiment [3]. It is clear from Fig. 1 that the atmospheric DBD is characterized by one current peak every half cycle of the voltage excitation, and the obvious periodicity of the current and voltage traces suggests that the generated plasma is temporally stable and repetitive. The discharge current density is about 9 $\mathrm{mA/cm}^2$ for the helium discharge, not dissimilar to 7.2 $\mathrm{mA/cm}^2$ measured in a comparable helium DBD experiment using a 10 kHz sinusoidal excitation voltage of 1.5 kV peak [3].

In the case of atmospheric DBD in pure nitrogen, we consider ionization, excitation, stepwise ionization, charge transfer, ionic conversions, and recombination. Our model includes 11 species; namely electrons, atomic nitrogen ions ($\mathrm{N}^+$), molecular nitrogen ions ($\mathrm{N}_2^+$, $\mathrm{N}_3^+$, and $\mathrm{N}_4^+$), molecular nitrogen metastables ($\mathrm{N}_2(\mathrm{a}^1\Sigma_\mathrm{u}^-)$, $\mathrm{N}_2(\mathrm{A}^3\Sigma_\mathrm{u}^+)$, $\mathrm{N}_2(\mathrm{B}^3\Pi_\mathrm{g})$, $\mathrm{N}_2(\mathrm{C}^3\Pi_\mathrm{u})$), and two ground state neutral species N atoms and $\mathrm{N}_2$ molecules. Secondary emission rate $\gamma$ is set to 0.01 for nitrogen [9] and Townsend ionization $\alpha$ is [9]

$$\alpha = A_1 p \exp\left(-B_1 \frac{p}{E}\right) \tag{3}$$

where $A_1 = 12\ \mathrm{cm}^{-1}\mathrm{torr}^{-1}$ and $B_1 = 342\ \mathrm{Vcm}^{-1}\mathrm{torr}^{-1}$ when $E/p$ is greater than $100\ \mathrm{Vcm}^{-1}\mathrm{torr}^{-1}$. Otherwise, $A_1 = 2.4\ \mathrm{cm}^{-1}\mathrm{torr}^{-1}$ and $B_1 = 155\ \mathrm{Vcm}^{-1}\mathrm{torr}^{-1}$. The diameter of the parallel-plate electrodes is 1.5 cm and the electrode separation distance is 0.2 cm. The alumina coating on both electrodes is 0.015 cm thick. These geometrical parameters are necessarily different from those for helium DBD to better match the breakdown characteristics of nitrogen. The transport parameters are identical to those used in [15]. Fig. 2 shows the current and voltage traces of stable nitrogen discharge with a 80 kHz applied voltage source of 6.5 kV. The discharge current density is approximately 300 $\mathrm{mA/cm}^2$, higher than that of the helium DBD. This is due to high external electric field and high reaction rates of the nitrogen DBD. Figs. 1 and 2 illustrate the typical current-voltage characteristics of stable DBD generated in atmospheric helium and nitrogen, respectively, when the excitation frequency is appropriately chosen. Now we investigate how current-voltage characteristics

Authorized licensed use limited to: LOUGHBOROUGH UNIVERSITY. Downloaded on August 26, 2009 at 09:23 from IEEE Xplore. Restrictions apply.

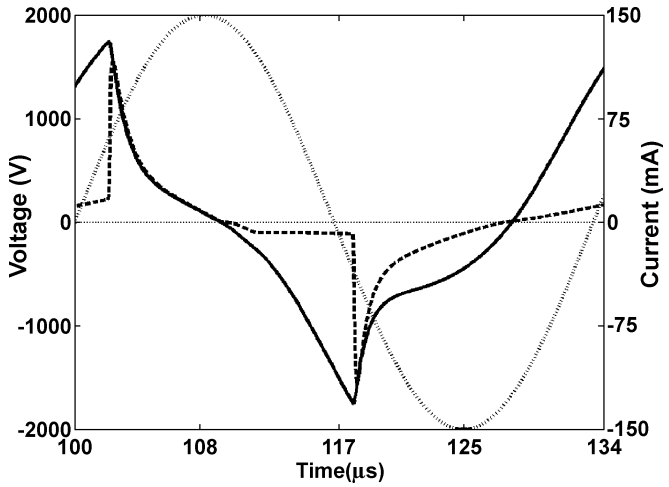


Fig. 1. Current and voltage characteristics of a helium-nitrogen DBD with 30 kHz sinusoidal excitation. The gas voltage is shown in the solid curve, the discharge current in the dashed curve, and the applied voltage in the dotted curve.

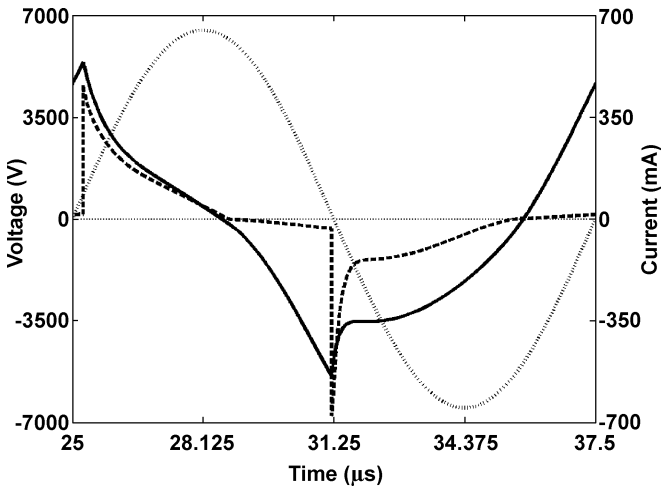


Fig. 2. Current and voltage characteristics of a nitrogen DBD with a 80 kHz sinusoidal excitation. The gas voltage is shown in the solid curve, the discharge current in the dashed curve, and the applied voltage in the dotted curve.

deviate from that in Figs. 1 and 2 when the excitation frequency is increased or decreased.

## III. Frequency Range of Stable DBD Generation

### A. Controlling Processes for Plasma Stability

To a large extent, the stable state of a glow discharge depends on fundamental processes that control electron production, removal, and spatial transfer. In the stable state, the production and loss processes of a gas discharge work together to achieve a dynamic balance in which the discharge has an obvious periodic characteristic. For atmospheric DBD, the memory voltage, $V_m$, across the two dielectric layers is central to this dynamic balance. It is induced by charge accumulation on the dielectrically coated electrodes and the charge accumulation is the result of ionization which occurred in the past. In other words, $V_m$ "memorizes" the previous discharge events. The dynamic balance of electron density in atmospheric DBD is critically related to the balance between the applied voltage, $V_a$, and $V_m$, across the two dielectric layers because they collectively determine the gas voltage

$$V_g = V_a - V_m \tag{4}$$

that controls directly electron production and plasma quenching. Before a discharge event, the rise of $V_a$ increases $V_g$ until the latter reaches the gas breakdown voltage resulting in significant electron production. Afterwards, the produced electrons are driven by $V_g$ toward the momentary anode, thus reversing the polarity of the initial memory voltage and eventually increasing the magnitude of $V_m$ in the direction that opposes to that of $V_a$ [3], [7]. As a result, a simultaneous rise of the applied voltage and the memory voltage keeps $V_g$ relatively unchanged yet above the breakdown voltage for a sustained period of gas discharge. For dielectric-barrier discharges, the dynamic balance between the applied voltage and the memory voltage is particularly important.

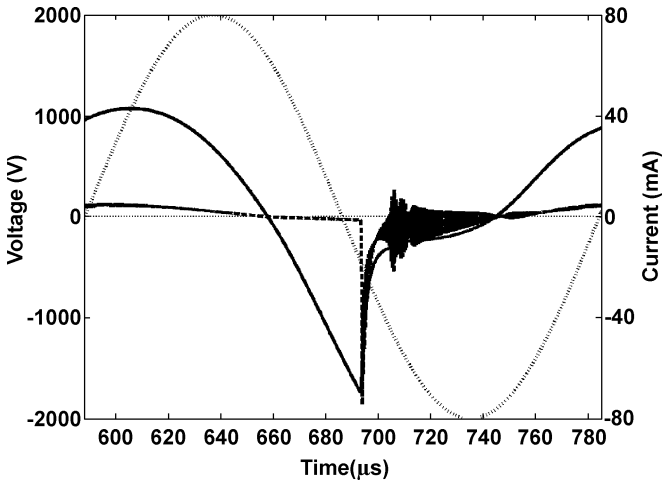


Fig. 3. Current and voltage characteristics of a helium–nitrogen DBD with a 5.1 kHz sinusoidal excitation. The gas voltage is shown in the solid curve, the discharge current in the dashed curve, and the applied voltage in the dotted curve.

When our numerical model is used to study current–voltage characteristics of the helium DBD with decreasing excitation frequency, the usual pattern of one discharge current peak every half-cycle in Fig. 1 gradually evolves to a new pattern of one current peak every one cycle and the peak value of the discharge current is also reduced. This change is illustrated with a 5.1 helium DBD in Fig. 3 where the discharge current peaks only in the negative half cycles of the applied voltage and its peak value is smaller. These observations suggest weakened electron production. During positive half cycles many small spikes are also observed on the current trace and again their small magnitude suggests the absence of significant electron production during positive half cycles. It is therefore evident that electron production is weakened at 5.1 kHz and may not be able to balance electron losses in the helium DBD. Indeed, when the excitation frequency is further reduced to below 5 kHz, stable helium DBD with temporally repetitive discharge current cannot be produced and the initial plasma is quenched within the first few cycles of excitation.

Authorized licensed use limited to: LOUGHBOROUGH UNIVERSITY. Downloaded on August 26, 2009 at 09:23 from IEEE Xplore. Restrictions apply.

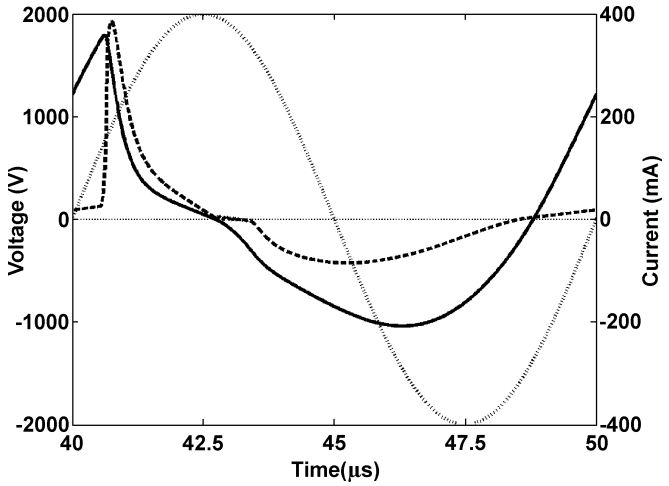


Fig. 4. Current and voltage characteristics of a helium-nitrogen DBD with a 100 kHz sinusoidal excitation. The gas voltage is shown in the solid curve, the discharge current in the dashed curve, and the applied voltage in the dotted curve.

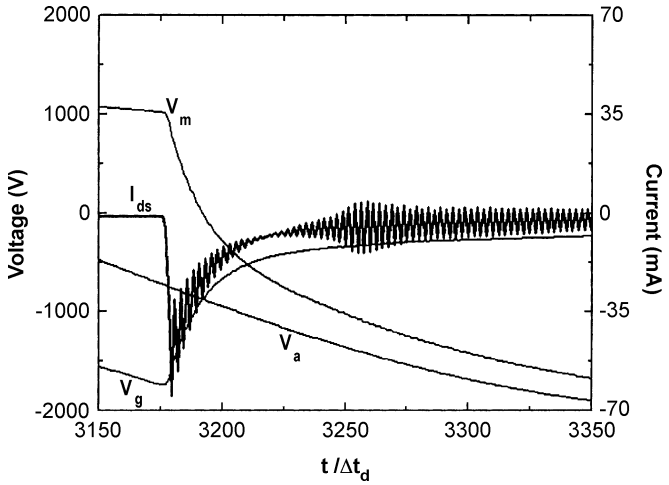


Fig. 5. The applied voltage, the memory voltage, the gas voltage and the discharge current as a function of time normalized to the electron drift time ($\Delta t_d = 158$ ns) at 5.1 kHz.

On the other hand, if the excitation frequency is increased from 30 kHz (see Fig. 1), the discharge current peaks in the negative half cycles of the excitation voltage reduce gradually and disappear eventually. This is illustrated with a 90 kHz helium DBD in Fig. 4. Interestingly the maximum discharge current in the 90 kHz case is higher than that in the 30 kHz case. For the helium DBD considered, the maximum excitation frequency for stable plasma production is 100 kHz. Therefore, the frequency range for the stable helium DBD is between 5 kHz and 100 kHz. It should be noted that this frequency range is specific to the geometrical parameters of the plasma rig and the nitrogen content (e.g., 0.5%) and as such should not be generalized. However, with different geometrical parameters and nitrogen contents, dynamic features of discharge current and voltage at the two ends of the frequency range are very similar to that in Figs. 3 and 4.

### *B. Stability Disruption Mechanism at Low Frequencies*

To unravel the reason why the helium DBD becomes unstable at frequencies below 5 kHz, it is useful to examine the time scale of electron charging of the dielectric coatings and that of the rise of the excitation voltage. These two timescales have to be comparable such that the memory voltage and the applied voltage are dynamically balanced to keep the gas voltage above the breakdown voltage. Electrons produced in the plasma bulk are driven to the momentary anode at the drift velocity, $v_d$. In helium, the electron mobility is $\mu = 10^6/p\ \mathrm{cm}^2/\mathrm{s}\cdot\mathrm{V}$ with $p$ being the gas pressure [9] and the maximum gas voltage in the 5.1 kHz case is approximately 1.7 kV (see Fig. 3). Therefore, the rms electric field over the 0.5 cm helium gap is $E_{\mathrm{rms}} = 2.40\ \mathrm{kV/cm}$ giving $v_d = \mu E_{\mathrm{rms}} = 3.16 \times 10^6\ \mathrm{cm/s}$. So it will take $\Delta t_d = 158\ \mathrm{ns}$ for an electron to travel from the cathode to the anode. Essentially, this is the timescale required for free electrons produced in the plasma bulk to sufficiently charge the dielectric coating of the electrodes in every half cycle of the excitation voltage. In turn, this is crucial for forming a substantial opposing electric field to control the rise of the applied voltage in the subsequent half cycle. It is desirable that the applied voltage rises at roughly the same speed as that of electron charging of the electrodes, since the simultaneous rise of $V_{\mathrm{m}}$ and $V_{\mathrm{a}}$ is particularly useful in keeping the gas voltage constant yet above the breakdown voltage according to (4). If we use $0.25T$ as a measure of the rise-time of the applied voltage with $T$ being its repetition period, this rise-time is about 50 $\mu$s at 5 kHz. In other words, the rise of the applied voltage is more than 300 times slower than the rise of the memory voltage. As a result, [and according to (4)], the gas voltage is above the breakdown voltage only briefly after which the much faster rise of the memory voltage reduces it rapidly to below the breakdown voltage. To confirm this, the applied and memory voltages are plotted in Fig. 5 over a short time-span around a discharge event. It is clear that the applied voltage rises much slower than the memory voltage thus leading to a rapid reduction of the gas voltage. The timescale mismatch of more than 300 times between the applied voltage and the memory voltage is very significant and it leads to a premature and permanent quenching of the helium DBD. The resulted reduction in electron production in turn disrupts the balance between electron production and loss for subsequent cycles of the excitation voltage. Below 5 kHz, this unbalancing becomes irreversible and makes it impossible to generate a stable DBD.

### *C. Stability Disruption Mechanism at High Frequencies*

When the excitation frequency is too high, it is possible that electrons produced in the plasma bulk are trapped between the two electrodes by the fast oscillating electric field of the applied voltage. Under such circumstances, most electrons cannot reach the electrodes and so they are unable to alter the memory voltage adequately. As a result, the memory voltage remains relatively unchanged and is unable to maintain a dynamic balance with the applied voltage [see (4)].

To evaluate this hypothesis, we consider electron oscillation under a sinusoidal electric field. If the excursion of most electrons from the midpoint between the two electrodes is less than half of the interelectrode distance, they will be unable to adequately charge the dielectrically coated electrodes and so the memory voltage cannot maintain a dynamic balance with the

Authorized licensed use limited to: LOUGHBOROUGH UNIVERSITY. Downloaded on August 26, 2009 at 09:23 from IEEE Xplore. Restrictions apply.

applied voltage for repetitive and stable generation of DBD. To this end, we estimate the oscillation amplitude of a charged particle in discharge plasma as [16]

$$x_m = \frac{\frac{eE_a}{m}}{\sqrt{\left(\omega^2 - \omega_p^2\left(\frac{2x_m}{L}\right)\right)^2 + \omega^2 v_m^2}} \tag{5}$$

where $e$ is the electron charge, $m$ mass of the charged particle, $E_a$ the electric field across the helium gap, $\omega$ the radian frequency of the applied voltage, $L$ the separation distance between two electrodes, and $v_{\rm m} = q/m\mu$ the collision frequency. $\omega_p$ is the plasma frequency given by

$$\omega_p = \sqrt{\frac{e^2 n_e}{\varepsilon_0 m}} = 5.65 \times 10^4 \sqrt{n_e(\mathrm{cm}^{-3})}\ \mathrm{s}^{-1}. \tag{6}$$

Here, $n_{\rm e}$ is the electron density spatially averaged across the interelectrode gap. Electron mobility in helium is $\mu_{\rm e} = 10^6/p\ \mathrm{cm^2 torr/(Vs)}$ [9] and the gas pressure $p = 760$ torr for our simulation. So the collision frequency of electrons is $v_{\rm me} = q/m_e\mu_{\rm e} = 1.34 \times 10^{12}\ \mathrm{s}^{-1}$. For helium ions, $m_{\rm i} = 6.64 \times 10^{-27}$ kg and the collision frequency is $6.8 \times 10^9\ \mathrm{s}^{-1}$ [2]. It is interesting to note that (5) is similar to the rms displacement of charged particles formulated in [2]

$$x_{rms} = \frac{2}{\pi}\frac{eE_a}{m\omega\nu_m} \tag{7}$$

if $|\omega^2 - \omega_p^2(2x_m/d)| \ll \omega v_m$. We have performed a number of numerical simulations for the helium DBD and found that $|\omega^2 - \omega_p^2(2x_m/d)| \ll \omega v_m$ is not true for electrons under atmospheric pressure. For example, if we assume $n_e = 10^{10}\ \mathrm{cm}^{-3}$ and $2x_m/L \approx 1$, $\omega_p = 5.65 \times 10^9\ \mathrm{s}^{-1}$. At 100 kHz, $|\omega^2 - \omega_p^2(2x_m/d)| \approx \omega_p^2 > \omega v_{me}$. Therefore, (5) should be used instead of (7).

Although (5) is derived for sinusoidal voltage and the gas voltage is not strictly sinusoidal (see Fig. 1), we use it as an approximation to estimate the amount of electron excursion normalized to $0.5L$. At 100 kHz, the peak gas voltage is approximately 2 kV and so the peak electric field $E_{\rm a} = 2\ \mathrm{kV}/0.5\ \mathrm{cm} = 4\ \mathrm{kV/cm}$. With this, (5) is solved for $2x_m/L$ and the results are shown in Fig. 6. For an electron located initially at the midpoint of the interelectrode space, Fig. 6 suggests that its excursion distance decreases with increasing excitation frequency. At 100 kHz, $2x_{\rm m}/L$ is less than 0.5 suggesting that the electron travels at most a quarter of the interelectrode distance during one half cycle. In other words, it is unlikely to reach the dielectrically coated electrodes. This supports strongly the hypothesis that the stability of atmospheric DBD is disrupted by electron trapping. Further evidence is found in the spatial distribution of the electron density at 100 kHz, which peaks in the central region of the interelectrode space for a very large portion of each cycle.

It is useful to compare the stability disruption mechanisms at both the low and the high frequency ends. At the low frequency end (5 kHz), the plasma stability is disrupted because the applied voltage increases too slowly with respect to the electron charging time of the dielectrically coated electrodes. This mismatched timescale causes the gas voltage to be reduced too quickly

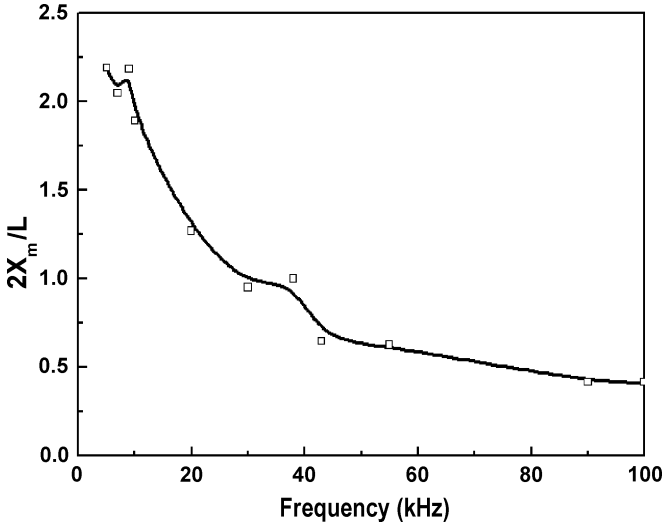


Fig. 6. Frequency dependence of the electron excursion distance normalized to half of the interelectrode distance.

leading to a premature plasma quenching. On the other hand, at the high frequency end (100 kHz) , most electrons produced in the plasma bulk are trapped and cannot reach the electrodes. As a result, the memory voltage is not increased sufficiently to counteract the rise of the applied voltage and to control the growth of the gas voltage [see (4)]. Although the specific reasons differ, both situations are associated with disruption of the dynamic balance between the applied voltage and the memory voltage. These plasma stability disruption mechanisms are specific for dielectric-barrier discharges, and may not be applicable to other nonthermal atmospheric discharges that do not rely on dielectrically coated electrodes such as RF and microwave atmospheric plasmas [17], [18].

### *D. Plasma Stability Disruption in Nitrogen DBD*

We perform similar numerical simulations for the pure nitrogen dielectric-barrier discharge described in Section III-A. The frequency range of plasma stability for this pure nitrogen DBD is found to be between 2 kHz and 705 kHz. It is also found that plasma stability disruption mechanisms are of the same nature in the nitrogen DBD as that in the helium DBD. One of the reasons why the nitrogen DBD has a much higher upper frequency bound is the much larger gas voltage and hence a greater electric field across the nitrogen gap. As shown in Fig. 2, the peak gas voltage is around 5.3 kV and so the maximum electric field is 26.5 kV/cm over the 0.2 cm nitrogen gap. In the case of the helium DBD, the peak gas voltage is 1.7 kV and the maximum electric field is 3.4 kV/cm across the 0.5 cm helium gap. Therefore, the electric field in the nitrogen DBD is almost 8 times that in the helium DBD. This larger electric field is important to drive electrons onto the electrodes at high frequencies and is largely responsible for the higher upper frequency bound in the nitrogen DBD.

### *E. Effects of Geometrical Parameters and Plasma Chemistry*

There are at least three key geometrical parameters that affect discharge dynamics significantly, and they are: 1) the electrode

Authorized licensed use limited to: LOUGHBOROUGH UNIVERSITY. Downloaded on August 26, 2009 at 09:23 from IEEE Xplore. Restrictions apply.

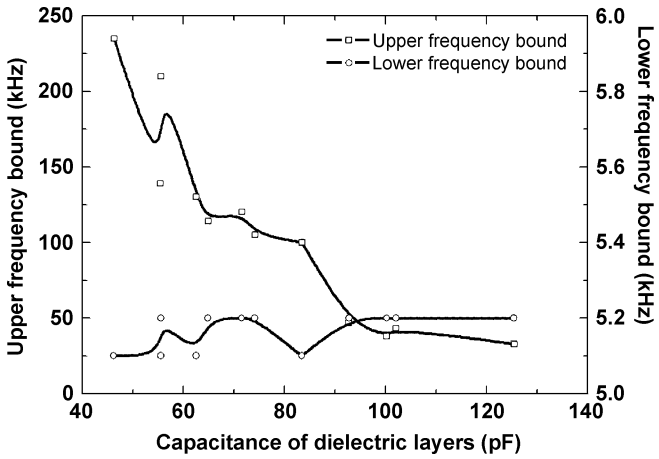


Fig. 7. Lower and upper frequency bounds at different barrier capacitance.

diameter, 2) the thickness of the dielectric barrier, and 3) permittivity of the dielectric barrier. Since our numerical code is one-dimensional, the effect of the electrode diameter cannot be explored adequately. Our experimental work shows that the electrode diameter can affect crucially the uniformity of the generated plasma and indeed its glow-to-arc transition [19]. However, multi-dimensional simulation must be performed before one can understand how the electrode diameter may affect the lower and upper frequency bounds. One the other hand, numerical examples suggest that both the thickness and permittivity of the dielectric barrier affect the lower and upper frequency bounds. Interestingly, their effects are well represented by that of the barrier capacitance on the lower and upper frequencies as shown in Fig. 7. As the barrier capacitance increases, either through increase in permittivity or through reduction in barrier thickness, the upper frequency decreases while the lower frequency changes little.

We have already established that the upper frequency bound is due to electron trapping. In other words, the applied voltage must vary sufficiently slowly to allow for an adequate portion of free electrons in the plasma bulk to reach the dielectrically coated anode such that these electrons can then cause sufficient change in the memory voltage for future ionization. When the barrier capacitance increases, more electrons are needed in order to induce the same change in the memory voltage because $\Delta Q = C\,\Delta V_m$. To allow for more electrons to reach the instantaneous anode, the applied voltage has to vary more slowly. Therefore, the upper frequency reduces as the barrier capacitance increases. On the other hand, the lower frequency bound is due to the mismatch between the electron drift time and the half period of the applied voltage. These two parameters are not affected by the barrier capacitance and therefore, the lower frequency remains relatively unchanged.

Another obvious geometrical parameter is the electrode gap distance. Numerical examples suggest that as the electrode gap increases both the lower frequency and upper frequency bounds decrease. At low frequencies, a larger electrode gap increases the electron drift time and so the applied voltage can vary more slowly without causing too much mismatch between its half period and the electron drift velocity. In other words the lower frequency bound becomes smaller. At high frequencies, a larger

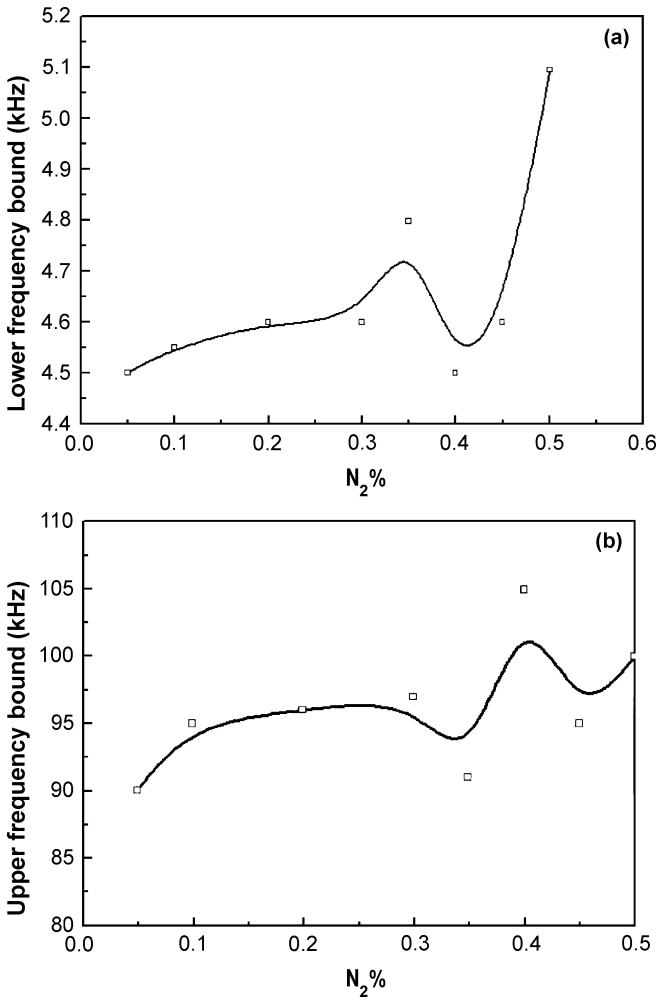


Fig. 8. Dependence of the lower and upper frequency bounds on the nitrogen percentage in the gas mixture of the helium DBD.

electrode gap makes it easier to trap electrons at any given frequency and as such the upper frequency bound must decrease to avoid too much electron trapping.

To explore the effect of plasma chemistry, we note that both the lower and the upper frequency bounds are extended when the background gas is changed from helium-nitrogen to nitrogen. Also, we simulate the helium DBD with the nitrogen content between 0.05% and 0.5%, and find that both the lower and the upper frequency bounds change markedly as shown in Fig. 8. As the nitrogen content increases, the Penning ionization is progressively enhanced [7] as confirmed numerically by increment of the electric field. At low frequencies, the increase of the electric field from 3.7 kV/cm at 0.3% nitrogen to 4.9 kV/cm at 0.5% nitrogen accelerates the electron drift toward the instantaneous anode and as a result the applied voltage must change faster in order to react to the change of the memory voltage. Therefore, the lower frequency bound increases as the nitrogen content increases and this is shown in Fig. 8(a). At high frequencies on the other hand, the increase of the electric field from 3.6 kV/cm at 0.3% nitrogen content to 4.6 kV/cm increases the electron displacement [see (7)] and as such relieve the degree of electron trapping. This in turn, allows for an increase in the upper frequency bound, as clearly suggested in Fig. 8(b). It is therefore

Authorized licensed use limited to: LOUGHBOROUGH UNIVERSITY. Downloaded on August 26, 2009 at 09:23 from IEEE Xplore. Restrictions apply.

evident that plasma chemistry impacts significantly on the specific range of the excitation frequency for plasma stability.

## IV. Conclusion

Plasma stability of nonthermal atmospheric dielectric-barrier discharges has been studied under different frequencies of sinusoidal excitation. Through numerical simulation, it was shown that the frequency range of plasma stability is from 5 kHz to 100 kHz for a helium-nitrogen DBD and from 2 kHz to 705 kHz for a pure nitrogen DBD. Stability disruption mechanisms were also studied for these two atmospheric DBD. It was found that the mismatch of the rise time between the memory voltage and the applied voltage became irreversibly too large when the excitation frequency was too low (5 kHz for the helium DBD and 2 kHz for the nitrogen DBD). This mismatch leads to a too-large memory voltage compared to the applied voltage, and as such the gas voltage is rapidly reduced leading to a premature plasma quenching. On the other hand, electrons produced in the plasma bulk became trapped in the interelectrode gap without being able to reach the electrodes if the excitation frequency was too high. As a result, the memory voltage increases little and is unable to maintain a dynamic balance with the applied voltage. This also leads to premature plasma quenching. These two stability disruption mechanisms were confirmed for both the helium DBD and the nitrogen DBD, and are therefore generic. They offer additional insight into the fundamental mechanisms for stable generation and operation of atmospheric glow discharges particularly nonthermal atmospheric DBD. In addition, the frequency range established for plasma stability will allow informed choice of power sources from commercial products for DBD production and facilitate design considerations for optimized and future power sources. Ultimately, this generic dependence will contribute to system optimization of atmospheric dielectric-barrier discharge devices with tailored characteristics for DBD dynamics and for power source matching.

## References


[1] E. E. Kunhardt, "Generation of large-volume, atmospheric-pressure, nonequilibrium plasmas," *IEEE Trans. Plasma Sci.*, vol. 28, pp. 189–200, Feb. 2000.

[2] J. R. Roth, *Industrial Plasma Engineering*. Bristol, U.K.: Inst. Physics, 2002, vol. 2.

[3] F. Massines, A. Rabehi, P. Decomps, R. Gadri, P. Segur, and C. Mayoux, "Experimental and theoretical study of a glow discharge at atmospheric pressure controlled by dielectric barrier," *J. Appl. Phys.*, vol. 83, pp. 2950–2957, Mar. 1998.

[4] T. Yokoyama, M. Kogoma, T. Moriwaki, and S. Okazaki, "The mechanism of the stabilization of glow plasmas at atmospheric pressure," *J. Phys. D: Appl. Phys.*, vol. 23, pp. 1125–1128, Aug. 1990.

[5] S. Okazaki, M. Kogoma, M. Uehara, and Y. Kimura, "Appearance of stable glow discharge in air, argon, oxygen and nitrogen at atmospheric pressure using a 50 Hz source," *J. Phys. D: Appl. Phys.*, vol. 26, pp. 889–892, May 1993.

[6] F. Tochikubo, T. Chiba, and T. Watanabe, "Structure of low-frequency helium glow discharge at atmospheric pressure between parallel plate dielectric electrodes," *Jpn. J. Appl. Phys.*, vol. 38, pp. 5244–5250, Sep. 1999.

[7] M. G. Kong and X. T. Deng, "Electrically efficient production of a diffuse nonthermal atmospheric plasma," *IEEE Trans. on Plasma Sci.*, vol. 31, pp. 7–18, Feb. 2003.

[8] J. J. Shi and M. G. Kong, "Cathode fall characteristics in a DC atmospheric pressure glow discharge," *J. of Appl. Phys.*, vol. 84, no. 9, pp. 5504–5513, Sept. 2003.

[9] Y. Raizer, *Gas Discharge Physics*. Berlin, Germany: Springer, 1997.

[10] S. V. Patankar, *Numerical Heat Transfer and Fluid Flow*. Bristol, PA: Hemisphere, 1980.

[11] Y. B. Golubovskii, V. A. Maiorov, J. Behnke, and J. F. Behnke, "Influence of elementary processes over an homogeneous barrier discharge in helium," in *Proc. 8th Int. Symp. High Pressure Low Temperature Plasma Chemistry*, vol. 1, Tartu, Estonia, 2002, pp. 48–52.

[12] P. Segur, F. Massines, A. Rabehi, and M. C. Bordage, "Theoretical and experimental analysis of a high pressure glow discharge controlled by a dielectric barrier," in *Gaseous Dielectric Conference*, Virginia Beach, VA, 1998.

[13] A. L. Ward, "Calculations of cathode-fall characteristics," *J. Appl. Phys.*, vol. 33, pp. 2789–2794, Sep. 1962.

[14] F. Young and C.-H. J. Wu, "Two-dimensional, self-consistent, three-moment simulation of RF glow discharges," *IEEE Trans. Plasma Sci.*, vol. 21, pp. 312–321, June 1993.

[15] P. Segur and F. Massines, "The role of numerical modeling to understand the behavior and to predict the existence of an atmospheric pressure glow discharge controlled by a dielectric barrier," in *Gas Discharge 2000*, Glasgow, U.K., 2000, p. IL3.

[16] Y. Raizer, M. N. Shneider, and N. A. Yatsenko, *Radio-Frequency Capacitive Discharge.*. Boca Raton, FL: CRC, 1995.

[17] A. Schutze, J. Y. Jeong, S. E. Babayan, J. Park, and G. S. Selwyn, "The atmospheric-pressure plasma jet: a review and comparison to other plasma sources," *IEEE Trans. Plasma Sci.*, vol. 26, pp. 1685–1694, Dec. 1998.

[18] M. J. Shenton and G. C. Stevens, "Optical emission from atmospheric pressure nonequilibrium plasma," *IEEE Trans. Plasma Sci.*, vol. 30, pp. 184–185, Feb. 2002.

[19] J. J. Shi, X. T. Deng, R. Hall, J. D. Punnett, and M. G. Kong, "Three modes in a dc atmospheric pressure glow discharge," *J. Appl. Phys.*, vol. 84, no. 10, pp. 6303–6310, Oct. 2003.



**Xu Tao Deng** (S'01) was born in Shenzhen, China, in 1975. She received the B.Sc. degree in electronic engineering from Shenzhen University, in 1997, and the M.Sc. degree in telecommunications engineering from Liverpool University, Liverpool, U.K., in 1998. She is currently working toward the Ph.D. degree at Loughborough University, Leicestershire, U.K.

Her current research interests are atmospheric pressure glow discharges and their applications.

Ms. Deng is an Associate Member of the IEE.



**Michael G. Kong** (M'94–SM'98) received the B.Sc. and M.Sc. degrees, in electronics engineering, from Zhejiang University, Hangzhou, China, in 1984 and 1987, respectively, and the Ph.D. degree in electrical engineering from Liverpool University, Liverpool, U.K., in 1992.

He is a Senior Lecturer at Loughborough University, Leicestershire, U.K., where he also heads its Power and Renewable Energy Division. He is a committee member of the Ion and Plasma Surface Interaction Group at the Institute of Physics, U.K. He has been actively involved in research on nonthermal atmospheric gas discharges, compact waveguide free electron lasers, and power systems and devices. In these subject areas, he has published some 80 papers in scientific journals and peer-reviewed conference proceedings.


Authorized licensed use limited to: LOUGHBOROUGH UNIVERSITY. Downloaded on August 26, 2009 at 09:23 from IEEE Xplore. Restrictions apply.